The Complex Role of Multivalency in Nanoparticles Targeting the Transferrin Receptor for Cancer Therapies

Jin Wang[1,†], **Shaomin Tian**[1,†], **Robby A. Petros**[1,*], **Mary E. Napier**[1], and **Joseph M. DeSimone**[1,2,3,4,‡]

[1]Department of Chemistry and Carolina Center of Cancer Nanotechnology Excellence, University of North Carolina, Chapel Hill, NC 27599

[2]Department of Pathology, University of North Carolina, Chapel Hill, NC 27599

[3]Department of Pharmacology and Lineberger Comprehensive Cancer Center, University of North Carolina, Chapel Hill, NC 27599

[4]Department of Chemical and Biomolecular Engineering, North Carolina State University, Raleigh, NC 27695

Abstract

Transferrin receptor (TfR, CD71) has long been therapeutic target due to its over-expression on many malignant tissues. In this study, PRINT® nanoparticles were conjugated with TfR ligands for targeted drug delivery. Cylindrical poly(ethylene glycol)-based PRINT nanoparticles (diameter [d] = 200 nm, height [h] = 200 nm) labeled with transferrin receptor antibody (NP-OKT9) or human transferrin (NP-hTf), showed highly specific TfR-mediated uptake by all human tumor cell lines tested, relative to negative controls (IgG1 for OKT9 or bovine transferrin (bTf) for hTf). The targeting efficiency was dependent on particle concentration, ligand density, dosing time and cell surface receptor expression level. Interestingly, NP-OKT9 or NP-hTf showed little cytotoxicity on all solid tumor cell lines tested but were very toxic to Ramos B-cell lymphoma, whereas free OKT9 or hTf was not toxic. There was a strong correlation between TfR ligand density on particle surface and cell viability and particle uptake. NP-OKT9 and NP-hTf were internalized into acidic intracellular compartments but were not localized in EEA1 enriched early endosomes or lysosomes. Elevated caspase 3/7 activity indicates activation of apoptosis pathways upon particle treatment. Supplementation of iron suppressed the toxicity of NP-OKT9 but not NP-hTf, suggesting different mechanisms by which NP-hTf and NP-OKT9 exerts cytotoxicity on Ramos cells. Based on such an observation, the complex role of multivalency in nanoparticles is discussed. In addition, our data clearly reveal that one must be careful in making claims of "lack of toxicity" when a targeting molecule is used on nanoparticles and also raise concerns for unanticipated off-target effects when one is designing targeted chemotherapy nano-delivery agents.

I. Introduction

Transferrin (Tf) binds to iron and transports iron to virtually all tissues through the transferrin receptor (TfR, CD71) which is located on cell surfaces.[1] In addition to iron transportation and regulation of cell growth, Tf also appears to have an iron independent role in the immune system.[2] Studies have shown that TfR is highly expressed on proliferating normal cells and cancerous cells compared to resting cells, probably due to the elevated need of iron as a cofactor for DNA synthesis. Due to its differential expression in normal and malignant tissues, TfR has long been a target of pharmacological intervention.[3] Cytotoxic transferrin receptor antibodies (TfR mAb) have been widely studied for cancer treatment especially for tumors associated with the immune system.[2] Transferrin and transferrin receptor antibodies have also been used for site-specific drug delivery for various systems, including protein toxin conjugates, polymer drug conjugates, modified viral vectors, liposomes/polyplexes, and nanoparticles (NPs), etc.[4-5] Two types of liposomal formulations for targeted drug/gene delivery, MBP-426 and SGT-53 which are currently under Phase I clinical trials, utilize transferrin and an anti-transferrin receptor single-chain antibody fragment as targeting moieties, respectively.[6] Transferrin conjugated cyclodextrin polymer-based NPs, CALAA-01, developed by Davis et al. achieved the most success in the targeted delivery of small interfering RNA (siRNA)[7-9] and are undergoing a Phase I clinical trial.[10]

One of the common features for targeted polymer/liposome/NP based drug nanocarriers is the ability to attach multiple targeting ligands (i.e. multivalency) to achieve high avidity to the target cells of interest.[11-15] This is also the fundamental basis for sensitive NP based DNA diagnostics and biosensors.[16] Cheng et al. reported an increased binding affinity of cyclic RGD monomer, dimer, and tetramer for $\alpha_v\beta_3$ integrin due to multivalency.[17] The effect of multivalency has been widely applied to improve antibody therapeutics. However, modulating cell biology by using nanomaterials with multivalent surface ligands has largely been overlooked, and there are only a few precedents in the literature to the best of our knowledge.[18-19] Intercellular adhesion molecule 1 (ICAM-1), up-regulated in many pathologies, is a good target for intraendothelial drug delivery. Muro et al. discovered that although endothelial cells do not internalize free anti-ICAM-1 antibodies, NPs bearing multiple copies of ICAM-1 antibody can readily enter endothelial cells through receptor mediated endocytosis.[20] Two recent studies demonstrated that conjugating Herceptin® (Trastuzumab), an FDA approved monoclonal antibody to treat HER2+ breast cancer, to gold NPs[21] or liposomes[22] can enhance the toxicity to HER2 positive cells compared to free Herceptin. In general, the use of a multivalent targeting strategy reported for Herceptin is transforming the approach researchers are taking for the design of more efficacious and safe therapeutic agents. On the other hand, the potential perturbation of cell biology by multivalent targeting ligands on nanomaterials may also pose safety concerns for biomedical application of nanotechnology and impede its clinical use, which makes it necessary to evaluate the multivalent effect on cell biology and nanotoxicology.

In this study, we will discuss the complex role of multivalency in nanoparticles. Multivalent targeted NPs can not only boost avidity to targeted cell surface receptors as many have reported, but also, in certain cases, can derive toxicity from its multivalency where the monovalent free form of the targeting ligand itself is not toxic and where the ligand-free particle itself is also not toxic nor does it contain any added therapeutic cargo. We will demonstrate the potential of a new nanotechnology strategy in cancer treatment by converting human transferrin, the fourth most abundant serum protein in humans[1], into a potential therapeutic agent using PRINT® technology[23-24] for an aggressive form of non-Hodgkin's lymphoma. Due to the ubiquitous nature of transferrin in humans, transferrin-conjugated PRINT NPs will be expected to be less immunoresponsive compared to multivalent monoclonal antibodies.

II. Results and Discussions

II.1. Fabrication of Transferrin Receptor Targeted PRINT Nanoparticles

Researchers use an extremely wide range of fabrication techniques in order to produce nano-structures. Two main nano-fabrication techniques are the "bottom-up" strategy, in which nanostructures are constructed from molecules or atoms, and the "top-down" strategy, in which material is added or removed from a surface. As a top-down strategy, the PRINT technology developed in our group enables independent control over particle size, shape, surface chemistry and composition and provides a convenient approach for systematically tailoring the chemical composition of the NPs without changing the size, shape and dynamics of the particle which often plagues other particle technologies, especially those derived from self-assembly approaches when one adjusts the chemical composition.[23‾26] The PRINT process has been described previously[23‾26] and is schematically illustrated in Figure 1. Photocurable highly fluorinated perfluoropolyether (PFPE) elastomers are used as the molding material to replicate the features from a silicon master which is fabricated by photolithography technique. A pre-particle solution, which can be monomers, polymers, or pure biological molecules, is applied on the PFPE mold. A high surface energy sheet (i.e. polyethylene terephthalate (PET) sheet) is laminated onto the low surface energy PFPE mold and run through a pressured nip. The cavities on the mold are filled by the pre-particle solution in this step. The PET sheet is then peeled off from the mold. Due to the surface energy difference between the PFPE mold and the PET sheet, all the excess pre-particle solution adheres to the PET sheet. This is the key to forming "flash-free" isolated particles. [23] The pre-particle solution is solidified via photo-polymerization and curing of the pre-particle solution. The formed particles are then transferred to a sacrificial adhesive layer, which can be dissolved to release the PRINT particles.

Cylindrical particles (d = 200 nm, h = 200 nm) with a biocompatible poly(ethylene glycol) based composition were fabricated (Figure 2a and Supporting Information (SI), Table S1), which contained 20 wt% of 2-aminoethyl methacrylate for post-functionalization and 2 wt% of fluorescein o-acrylate conjugated to the matrix of the NPs to facilitate the tracking of the particles in cells. The PRINT nanoparticles fabricated, designated as NP-NH$_2$, have a hydrodynamic diameter of 287 ± 32 nm and with a very narrow polydisperspisity (PDI=0.015) based on dynamic light scattering measurements (Table 1). Due to the amine suface functionality, NP-NH$_2$ is positively charged with a ζ-potential of +39.9 ± 1.7 mV. The surface of NP-NH$_2$ was post-functionalized with human holo-transferrin (hTf), a negative control ligand based on bovine holo-transferrin (bTf) which does not crossreact with human TfR (Figure 2b),[27] anti-TfR monoclonal antibody OKT-9, or a control mouse antibody of the same isotype (IgG1, clone P3) (Figure 2c). The hydrodynamic diameters of the protein-conjugated NPs (NP-hTf, NP-bTf, NP-OKT9 and NP-IgG1) were ~300 nm and they all had similar negative ζ-potentials (~ – 30 mV, Table 1) to avoid non-specific cell uptake.[28] For both the targeted NPs and their controls, it was estimated that there were ~1200 targeting ligands on the surface of each NP based on BCA protein quantification assays (refer to the experimental section for details).

II.2. Targeting PRINT NPs to Transferrin Receptor on Cancer Cells

Six tumor cell lines (HeLa, Ramos, H460, SK-OV-3, HepG2 and LNCaP) which all over-express TfR on the cell surface and a transformed normal human cell line (HEK 293) that expresses very low levels of TfR (SI, Figure S1) were dosed with the TfR targeted NPs (NP-hTf and NP-OKT9) and their corresponding control NPs (NP-bTf and NP-IgG1) at a particle concentration of 100 μg/mL for 4 h at 37 °C. Flow cytometry was performed to quantify the percentage of cells that internalized the targeted NPs. As shown in Figure 3a, all the cancer cells employed in this study showed at least 80% of cell uptake for NP-hTf and NP-OKT9,

i.e., above 80% of the cells contained particles under this condition. In contrast, little cell uptake (< 10%) was observed for NP-bTf and NP-IgG1. This is not unexpected as we have previously shown that PRINT NPs with a negative zeta potential can have a dramatically lower internalization percentage in non-phagocytic cells relative to their positively charged analogues having the same sizes and shapes.28 It is interesting to note that HEK293 cells, which express low levels of TfR also achieved a significant accumulation of NP-hTf and NP-OKT9 (~65%) after 4 h dosing with a PRINT NP concentration of 100 μg/mL.

A kinetic study of cell uptake was performed with four cell lines that express TfR at different levels: Ramos > HeLa ≈ H460 > HEK293 (SI, Figure S1). Cells were dosed with NPs for 20, 60, 120 or 240 min at 37 °C. The uptake of PRINT NP conjugated with hTf increased with incubation time and the uptake rate clearly followed the trend of Ramos > HeLa ≈ H460 > HEK293 (Figure 4a), which correlates well to the TfR expression level on these cell lines. The control particle NP-bTf, on the other hand, was not internalized to an appreciable level (< 5%). A similar trend of cell uptake kinetics was also observed for NP-OKT9 (Figure 4b) versus the control NP-IgG1. Thus, for targeted delivery purpose, transferrin and transferrin receptor antibody can discriminate tumor cells from normal cells.

The cellular uptake of NP-hTf by Ramos could be suppressed by addition of hTf in a dose-dependent manner but not by addition of bovine transferrin, which does not react with human TfR (Figure 5a). A similar inhibition behavior was also observed for a transferrin targeted cyclodextran delivery system.8,29 Similarly, the cell uptake of NP-OKT9 by Ramos cells can also be suppressed by addition of free OKT9 monoclonal antibody in a dose-dependent manner but not by the addition of the mouse IgG1 isotype control antibody (Figure 5b). The dose-dependent inhibition of Ramos cell uptake of NP-hTf and NPOKT9 by their corresponding free targeting ligands indicates that transferrin receptors are responsible for the NP internalization. Thus, our data strongly argue that TfR is a good cancer target for drug delivery: NP-hTf and NP-OKT9 both showed highly specific transferrin receptor mediated cell uptake on a variety of cancer cells compared to the corresponding control NPs.

II.3. Cytotoxicity of the Transferrin Receptor Targeted PRINT Nanoparticles to Ramos Cells

The viability of the cells treated with the various targeted NPs was evaluated by using an MTS assay or measuring ATP generation in cells. Neither NP-hTf nor NP-OKT9 showed appreciable toxicity to the solid tumor cell lines (i.e. HeLa, H460, SK-OV-3, HepG2 and LNCaP) tested at a NP concentration of 100 μg/mL (Figure 3b). Thus, these hTf and OKT9 conjugated PRINT NPs can be considered as useful as targeted cancer imaging agents or a platform for the targeted delivery of chemotherapy agents (e.g. by adding small molecule cytotoxins or cytotoxic biologicals like certain siRNAs as cargos that could be released upon cell internalization) to these cancer cells.

However, and to our surprise, both NP-hTf and NP-OKT9 showed dose-dependent toxicity on Ramos cells even though no chemotherapeutics were incorporated as a cargo in the PRINT NPs. More than 70% of the Ramos cells treated with NP-hTf or NP-OKT9 died after 72 h at a NP concentration of 100 μg/mL (Figure 3b). In contrast, Ramos cells treated with NP-bTf or NP-IgG1 showed 100% viability within experimental error. And free hTf or OKT9 did not display cytotoxicity to Ramos cells, either (SI, Figure S2). The observation of low toxicity of the control NPs and the free targeting ligands (i.e. hTf and OKT9) suggests that the death of Ramos cells induced by NP-hTf and NP-OKT9 is due to the multivalent presentation of the NP surface ligands instead of non-specific toxicity of these NPs or the free targeting ligands.

Using multivalent targeting systems, including dimers, trimers, and multimers, has been a successful strategy for enhancing the avidity and/or biofunctions of proteins/peptides, especially for antibodies. Depending on the size of a particular nanoparticle system, hundreds to thousands of ligands can be conjugated to the surface of NPs, which should increase the avidity of the particles to the desired cell type, and potentially lead to increased efficacy. For example, Trastuzumab, an engineered antibody for Her2+ breast cancer therapy, showed an increase of potency up to 25 times upon conjugation to liposomes.[22]

The inhibition of tumor growth by anti-TfR antibodies was first reported in the 1980s[30⁻32] and has been extensively reviewed.[1] Multivalent TfR antibodies have also shown increased antitumor responses. Trowbridge and Lopez developed an IgA mAb against hTfR, designated 42/6, which blocked the binding of Tf to its receptor and inhibited the growth of a T-cell leukemic cell line.[31] R17 208 and REM.17, two IgM antibodies against the mouse TfR, were also reported to possess anti-proliferative activities by blocking the internalization of the TfR-Tf complex, which is one of main pathways for iron supplement in cells, resulting in iron depletion and proliferation inhibition.[33] Another two murine anti-human TfR IgG antibodies (OKT9 and B3/25) did not show significant cell growth inhibitory effects unless crosslinked with secondary Abs.[32,34] The data indicate that polymeric antibodies, such as anti-TfR IgA and IgM and anti-TfR IgGs crosslinked with a secondary antibodies, are required to inhibit cell proliferation by preventing internalization of the TfR-Tf complex. The Penichet group developed an anti-TfR IgG3-avidin fusion protein, which exhibited a strong growth inhibitory activity against a rat T-cell lymphoma cell line.[35] Interestingly, the anti-TfR IgG3 without the avidin tag did not inhibit any cell growth. It was discovered that due to the noncovalent interactions between the avidin tags, the anti-TfR IgG3-avidin fusion protein dimerized under native conditions. It was observed that the Penichet's antibody can be internalized with TfRs and the internalized TfRs travelled to endosomes and lysosmes and degraded intracellularly, which caused apoptosis and subsequent cell death. However, no matter which toxicity mechanism operates, all of the previous studies regarding TfR antibodies addressed the necessity for polymeric antibodies to induce inhibitory effect. The transferrin receptor targeted PRINT NPs have more than a thousand hTf or OKT9 on surface and are expected to achieve a similar multivalent effect.

II.3.1. Cell Uptake and Cytotoxicity of the TfR Targeted NPs as a Function of Surface Ligand Density—To understand the NP toxicity mechanism of these multivalent NPs for Ramos cells, the targeting ligand densities were varied on the NP surface by substituting the targeting ligands (i.e. hTf or OKT9) with their corresponding control ligands (i.e. bTf or IgG1) during the ligand conjugation process. NPs with different hTf density (0 %, 1 %, 5 %, 10 %, 25 % and 100 %) were incubated with Ramos cells for 4 h and as shown in Figure 6a, the level of Ramos cell uptake started to decrease when hTf density was lowered from 100 % to 10 %. The cell uptake of these PRINT NPs further decreased when the hTf density was lowered to 5% and 1%, and minimal cell uptake was observed when hTf was completely substituted with bTf. This may suggest that 25 % of the targeting ligand conjugated to the PRINT particles can achieve a similar extent of particle internalization as 100 % of targeting ligand. Similarly, NP-OKT9 also showed a ligand density dependent Ramos cell uptake (Figure 6c). It was also observed that the cell viability of the Ramos cell line depended on the hTf and OKT-9 surface ligand density as well (Figure 6b and 6d), which correlates to the ligand density dependent cell uptake (Figure 6a and 6c).

It was also observed that larger PRINT particles (5 μm), which are non-internalizable[28] and were surface-modified under the same reaction conditions as the 200 nm particles, showed little toxicity to the Ramos cells when conjugated with OKT-9 (SI, Figure S3). This observation together with the correlation between Ramos toxicity and NP cell uptake (Figure 6) suggests that the internalization of the targeted NPs is essential to achieve the

specific toxicity to Ramos cells. Thus, the growth inhibitory mechanism for these NPs is not due to preventing internalization of TfR-Tf complexes.

II.3.2. Internalization of the TfR Targeted NPs into Acidic Cellular Compartments

—Analysis using transmission electron microscopy (TEM) was carried out to visually confirm the intracellular internalization and localization of the PRINT particles. As expected, in Ramos cells treated with NP-hTf (Figure 7a, panels A and B) or NP-OKT9 (panels D and E), a large amount of particles can be observed being either surface associated with cells or trapped within intracellular vesicles. In contrast, few particles were observed in cells treated with the control NPs (Figure 7a, panels C and F).

To investigate the intracellular environment of cells containing the targeted NPs, the Ramos cells were treated with PRINT NPs that were labeled with DyLight 488 and were subsequently stained with Lysotracker® Red DND-99 which labels acidic compartments in live cells (Note: Lysotracker Red DND-99 is a cell-permeable pH sensitive fluorescent dye, which can label both *endosomes* and *lysosomes* indiscriminately). As shown in Figure 7b, green dye labeled NP-hTf and NP-OKT9 were co-localized with Lysotracker red in Ramos cells, indicating that the TfR-targeted NPs were internalized into an acidic environment. It is well known that TfR is recycled which matches its major physiological function as a shuttle in iron transportation. Internalized TfR, either free or in complex with iron-loaded transferrin, does not go through the endosome-lysosome pathway to avoid the degradation of TfR. And the endocytic vesicles formed by internalized TfR only transiently interacts with EEA-1 (early endosome antigen-1) enriched endosomes before going to juxtanuclear compartments and being recycled.[36] Similar to the TfR trafficking mechanism, we did not observe much co-localization of NP-hTf or NP-OKT9 with EEA-1 or LAMP-1 (lysosome associated membrane protein-1) enriched intracellular compartments in Ramos cells (SI, Figure S4). These data suggest that NP-hTf or NP-OKT9 stay in intracellular acidic compartments which do not express EEA-1 and LAMP-1.

Holo-Tf, upon binding to TfR, can be rapidly internalized by cells into acidic compartments, and after iron release the Tf-TfR complex is recycled to cell surface without going through endosome-lysosome pathway.[1] It has been reported that multivalent Tf (Tf_{10}) goes through a much slower trafficking and is selectively retained in endocytic recycling compartments. [37] Our data shows that NP-hTf was internalized by Ramos cells at a much slower rate than free hTf, probably due to the large size of particles. However, similar to free Tf, NP-hTf did not go to lysosomes but accumulated in acidic compartments that are free of EEA1 and LAMP1. It was also reported that in rabbit reticulocytes, transferrin-gold NP conjugates were exocytosed very slowly and accumulation of a large amount of gold NPs could be observed inside the cells, compared to the fast endocytosis and exocytosis of the Tf-TfR complex.[38] This much slower recycling of TfR may cause its degradation in the acidic environment and resulting in iron deprivation.

OKT9, on the other hand, binds to a different site on the transferrin receptor,[27] so OKT9 binding may not directly compete for cellular iron uptake through transferrin. However, OKT9 binding to K562 cells (erytholeukemia) results in rapid redistribution and enhanced degradation of TfR.[39] Like NP-hTf, NP-OKT9 also accumulated in non-endosome, non-lysosome acidic intracellular compartments of Ramos cells. Further study on the degradation and synthesis of TfR upon particle treatment should provide more conclusive information.

II.3.3. Apoptosis and Cytotoxic Mechanism of Ramos Cells Induced by the TfR-targeted Nanoparticles

—To determine whether the death of Ramos cells is through apoptotic pathways, caspase 3/7 activity of Ramos cells treated with the targeted NPs was measured. As shown in Figure 8a, Ramos cells treated with NP-hTf and NP-OKT9 at a

particle concentration of 200 μg/mL did not show appreciable caspase activity after 4 h incubation compared to the untreated cells. However, after 24 h of incubation, the caspase activity of Ramos cells treated with NP-hTf and NP-OKT9 increased by ~300 % and ~50 %, respectively. Ramos cells treated with NP-IgG1 showed basically no change in caspase activity at 4 or 24 h incubation. In addition, free human transferrin or free OKT-9 alone does not induce apoptosis of Ramos cells (Figure 8a).

In Penichet's study of the cell growth inhibition effect of the anti-TfR IgG3-avidin fusion protein, it was discovered that supplying ferric ammonium citrate (FAC) to the cells treated with the fusion protein dimer can relieve the cell growth inhibition effect, indicating that cell death was caused by iron deprivation.[40] A similar experiment was performed for NP-hTf and NP-OKT9 treated Ramos cells by supplementing the cells with 30 μM of FAC. As shown in Figure 8b, the toxicity effect of NP-OKT9 to the Ramos cells was fully suppressed with the addition of FAC, as demonstrated for the anti-TfR IgG3-avidin fusion protein dimer in Penichet's study,[40] which suggests that cell death triggered by NP-OKT9 may be mainly due to iron deprivation. In addition, it was found that compared to HeLa, H460 and LNCaP cells, Ramos cells were more sensitive to agents modulating iron metabolism pathways, such as EF-24, a curcumin analog which can modulate proteins of iron metabolism to achieve antitumor effects,[41⁻42] but statistically equally sensitive to other chemotherapeutics with different cytotoxic mechanisms, such as doxorubicin and Taxotere® (SI, Table S2). However, to our surprise, there was no change in the toxicity of NP-hTf to Ramos cells in the presence vs. absence of FAC, suggesting that the cytotoxcity of NP-hTf is not solely due to iron deprivation. NPs with multivalent hTf may trigger some additional profound cellular signals, which NP-OKT9 cannot trigger, to activate apoptosis of Ramos cells. Indeed, there has been some evidence that Tf and TfR have iron-independent roles in the immune system.[2] This is further supported by the observation that NP-hTf and NP-OKT9 were toxic to Ramos cells, a B cell lymphoma, but not to all other solid tumor cell lines employed in this study. Further analysis on the mechanisms of the targeted NP-triggered Ramos death is currently underway. The unexpected toxicity for Ramos cells from NP-hTf should also raise concern to the nano-bio community that multivalent targeting ligands with NPs can not only boost their cell avidity but may also cause unintended consequences in the target or non-targeted cells and tissues. Our data clearly reveal that one must be careful in making claims of "lack of toxicity" when a targeting molecule is used on nanoparticles. Extensive knowledge on how multivalent targeting ligands interact with cells, particularly with normal cells and tissues, is necessary to ensure safe biomedical application of nanotechnology.

III. Conclusions

We have shown that PRINT NPs conjugated with human transferrin or transferrin receptor monoclonal antibody can specifically target a broad spectrum of cancers, making it a useful platform for targeted drug delivery. And they were not toxic to the cancer cells studied except for Ramos cells. The cellular uptake level can be thoroughly modulated by adjusting surface ligand density. In addition, NP-hTf and NP-OKT9 can discriminate tumor cells from normal cells as shown by the kinetic study. Thus, these hTf and OKT9 conjugated PRINT NPs can be used as targeted cancer imaging agents or as a platform for targeted drug delivery to cancer cells. Accumulation of NP-hTf and NP-OKT9 into acidic intracellular vesicles instead of lysosomes makes TfR especially a good target for delivery of cargos that are sensitive to enzyme digestion in lysosomes, such as siRNA and proteins etc. Acid-labile biodegradable nanomaterials can still take advantage of the low pH in particle-containing vesicles, although the exact pH in these intracellular vesicles is still unavailable by current techniques.

More importantly, we have demonstrated a novel way to take advantage of the multivalent NPs to modulate cell biology: essentially non-toxic transferrin and transferrin receptor antibody OKT9 can be converted into potential cancer therapeutics by conjugation to PRINT NPs. These particles are selectively toxic to Ramos lymphoma cells but not to solid tumor cells or normal kidney cell tested here. Compared to the prevalent immunotherapy using antibodies, using human transferrin conjugated to NPs as a cancer therapy will be expected to cause minimal immunoresponses. This strategy may also be applied to other surface receptors and to other nanomaterials, such as gold NPs, quantum dots, liposomes etc, although PRINT technology is particularly advantageous over other fabrication processes in terms of using essentially any biodegradable and biocompatible materials to fabricate stable NPs. The unexpected toxicity for Ramos cells from the multivalent nanoparticles should also raise concern to the nano-bio community and help better design nanomedicines.

Supplementary Material

Refer to Web version on PubMed Central for supplementary material.

Acknowledgments

REFERENCES

1. Daniels TR, Delgado T, Rodriguez JA, Helguera G, Penichet ML. Clin Immunol. 2006; 121:144. [PubMed: 16904380]

2. Macedo MF, de Sousa M. Inflamm Allergy Drug Targets. 2008; 7:41. [PubMed: 18473900]

3. Li H, Qian ZM. Med Res Rev. 2002; 22:225. [PubMed: 11933019]

4. Daniels TR, Delgado T, Helguera G, Penichet ML. Clin Immunol. 2006; 121:159. [PubMed: 16920030]

5. Choi CHJ, Alabi CA, Webster P, Davis ME. Proc. Natl. Acad. Sci. USA. 2010; 107:1235. [PubMed: 20080552]

6. Heath JR, Davis ME. Annu. Rev. Med. 2008; 59:251. [PubMed: 17937588]

7. Heidel JD, Yu Z, Liu JY, Rele SM, Liang Y, Zeidan RK, Kornbrust DJ, Davis ME. Proc. Natl. Acad. Sci. USA. 2007; 104:5715. [PubMed: 17379663]

8. Bellocq NC, Pun SH, Jensen GS, Davis ME. Bioconjugate Chem. 2003; 14:1122.

9. Davis ME, Zuckerman JE, Choi CH, Seligson D, Tolcher A, Alabi CA, Yen Y, Heidel JD, Ribas A. Nature. 2010; 464:1067. [PubMed: 20305636]

10. Davis ME. Mol. Pharm. 2009; 6:659. [PubMed: 19267452]

11. Kang B, Mackey MA, El-Sayed MA. J Am Chem Soc. 2010; 132:1517. [PubMed: 20085324]

12. Byrne JD, Betancourt T, Brannon-Peppas L. Advanced drug delivery reviews. 2008; 60:1615. [PubMed: 18840489]

13. Escorcia FE, McDevitt MR, Villa CH, Scheinberg DA. Nanomed. 2007; 2:805.

14. Kabanov AV, Vinogradov SV. Angew Chem Int Ed Engl. 2009; 48:5418. [PubMed: 19562807]

15. Ogris M, Walker G, Blessing T, Kircheis R, Wolschek M, Wagner E. J Control Release. 2003; 91:173. [PubMed: 12932649]

16. Rosi N, Mirkin C. Chem. Rev. 2005; 105:1547. [PubMed: 15826019]

17. Cheng Z, Wu Y, Xiong Z, Gambhir SS, Chen X. Bioconjug Chem. 2005; 16:1433. [PubMed: 16287239]

18. Huang YF, Liu H, Xiong X, Chen Y, Tan W. J Am Chem Soc. 2009; 131:17328. [PubMed: 19929020]

19. Bowman MC, Ballard TE, Ackerson CJ, Feldheim DL, Margolis DM, Melander C. J Am Chem Soc. 2008; 130:6896. [PubMed: 18473457]

20. Muro S, Garnacho C, Champion JA, Leferovich J, Gajewski C, Schuchman EH, Mitragotri S, Muzykantov VR. Mol Ther. 2008; 16:1450. [PubMed: 18560419]

21. Jiang W, Kim BY, Rutka JT, Chan WC. Nat. Nanotechnol. 2008; 3:145. [PubMed: 18654486]

22. Chiu GN, Edwards LA, Kapanen AI, Malinen MM, Dragowska WH, Warburton C, Chikh GG, Fang KY, Tan S, Sy J, Tucker C, Waterhouse DN, Klasa R, Bally MB. Mol Cancer Ther. 2007; 6:844. [PubMed: 17339368]

23. Rolland J, Maynor B, Euliss L, Exner A, Denison G, DeSimone J. J. Am. Chem. Soc. 2005; 127:10096. [PubMed: 16011375]

24. Euliss L, DuPont J, Gratton S, DeSimone J. Chem. Soc. Rev. 2006; 35:1095. [PubMed: 17057838]

25. Kelly J, DeSimone J. J. Am. Chem. Soc. 2008; 130:5438. [PubMed: 18376832]

26. Zhang H, Nunes J, Gratton S, Herlihy K, Pohlhaus P, DeSimone J. New Journal of Physics. 2009; 11:075018.

27. Bártek J, Viklický V, Stratil A. Br. J. Haematol. 1985; 59:435. [PubMed: 2578807]

28. Gratton SEA, Ropp PA, Pohlhaus PD, Luft JC, Madden VJ, Napier ME, DeSimone JM. Proc. Natl. Acad. Sci. USA. 2008; 105:11613. [PubMed: 18697944]

29. Bartlett D, Davis M. Bioconj. Chem. 2007; 18:456.

30. Trowbridge I, Domingo D. Nature. 1981; 294:171. [PubMed: 6272120]

31. Trowbridge IS, Lopez F. Proc. Natl. Acad. Sci. USA. 1982; 79:1175. [PubMed: 6280171]

32. Lesley JF, Schulte RJ. Mol Cell Biol. 1985; 5:1814. [PubMed: 3018527]

33. White S, Taetle R, Seligman PA, Rutherford M, Trowbridge IS. Cancer Res. 1990; 50:6295. [PubMed: 2400993]

34. Taetle R, Castagnola J, Mendelsohn J. Cancer Res. 1986; 46:1759. [PubMed: 3004704]

35. Ng PP, Dela Cruz JS, Sorour DN, Stinebaugh JM, Shin SU, Shin DS, Morrison SL, Penichet ML. Proc. Natl. Acad. Sci. USA. 2002; 99:10706. [PubMed: 12149472]

36. Leonard D, Hayakawa A, Lawe D, Lambright D, Bellve K, Standley C, Lifshitz L, Fogarty K, Corvera S. J. Cell Sci. 2008; 121:3445. [PubMed: 18827013]

37. Marsh EW, Leopold PL, Jones NL, Maxfield FR. J Cell Biol. 1995; 129:1509. [PubMed: 7790351]

38. Fodor I, Egyed A, Lelkes G. Eur J Cell Biol. 1986; 42:74. [PubMed: 3792344]

39. Weissman AM, Klausner RD, Rao K, Harford JB. J Cell Biol. 1986; 102:951. [PubMed: 3005341]

40. Ng PP, Helguera G, Daniels TR, Lomas SZ, Rodriguez JA, Schiller G, Bonavida B, Morrison SL, Penichet ML. Blood. 2006; 108:2745. [PubMed: 16804109]

41. Jiao Y, Wilkinson J. t. Christine Pietsch E, Buss JL, Wang W, Planalp R, Torti FM, Torti SV. Free Radic Biol Med. 2006; 40:1152. [PubMed: 16545682]

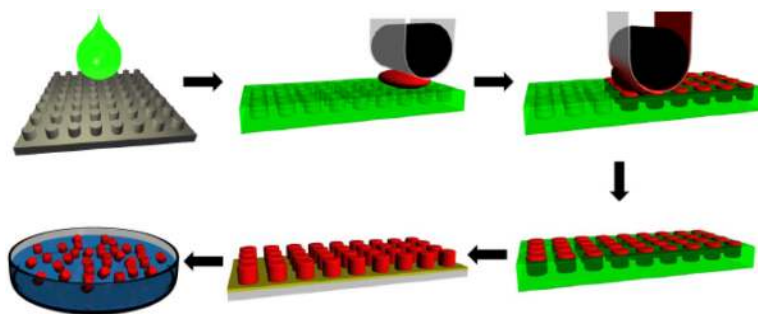42. Mosley CA, Liotta DC, Snyder JP. Adv Exp Med Biol. 2007; 595:77. [PubMed: 17569206]

Figure 1.
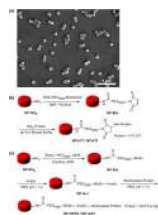PRINT nanoparticle fabrication process.

Figure 2.
PRINT nanoparticle characterization and post-functionalization. (a) scanning electron microscopy (SEM) image of PRINT nanoparticles (cylindrical, d = 200 nm, h = 200 nm). (b) Post-functionalizations of PRINT nanoparticles with human/bovine transferrin through lysine-maleimide reactions. (c) Post-functionalizations of PRINT nanoparticles with transferrin receptor monoclonal antibody OKT9 and its isotype control IgG1 through biotin-avidin strategies.
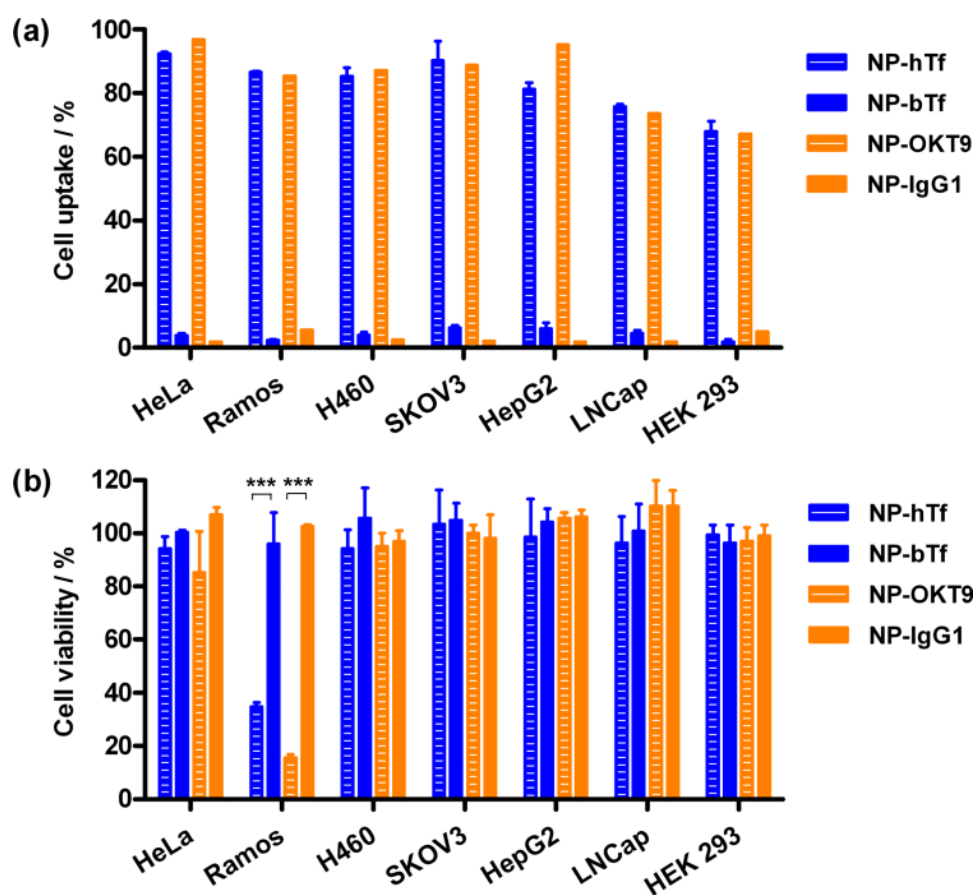
Figure 3.
Transferrin receptor-targeted delivery of PRINT nanoparticles to various cancer and non-cancer cell lines. (a) Cellular uptake and (b) cytotoxicity of particles. All the cells were dosed with 100 μg/ml fluorescein labeled NPs for 4 h at 37 °C and were collected for flow cytometry analysis after quenching the fluorescence of surface bound particles with trypan blue. For cytotoxicity assays, cells were further incubated at 37 °C for another 72 h before viability assays were performed. HeLa, cervical carcinoma; Ramos, Burkitt's B-cell lymphoma; H460, lung adenocarcinoma; SK-OV-3, ovarian adenocarcinoma; HepG2, hepatocellular carcinoma; LNCap, prostate adenocarcinoma; HEK 293, human embryonic kidney cell. Error bars represent standard deviations from triplicate wells. ***, P < 0.001.
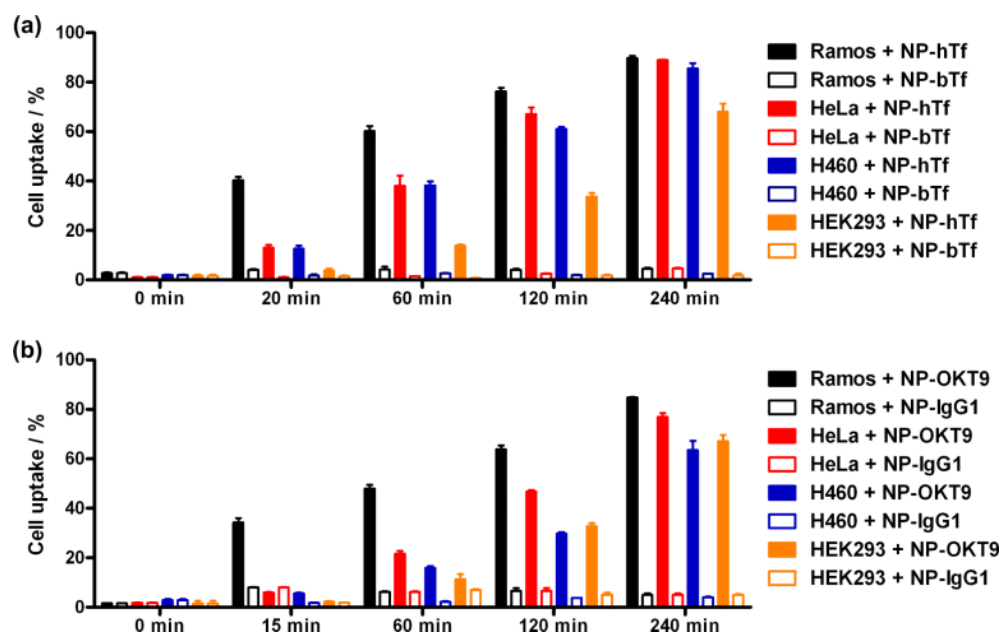
Figure 4.
Cell uptake kinetics of transferrin and transferrin receptor antibody conjugated particles on Ramos, HeLa, H460 and HEK293 cell lines. Cells were dosed with 100 µg/ml fluorescein labeled nanoparticles for indicated times at 37°C, then collected for flow cytometry analysis of cell uptake after quenching the fluorescence of surface bound particle with trypan blue.
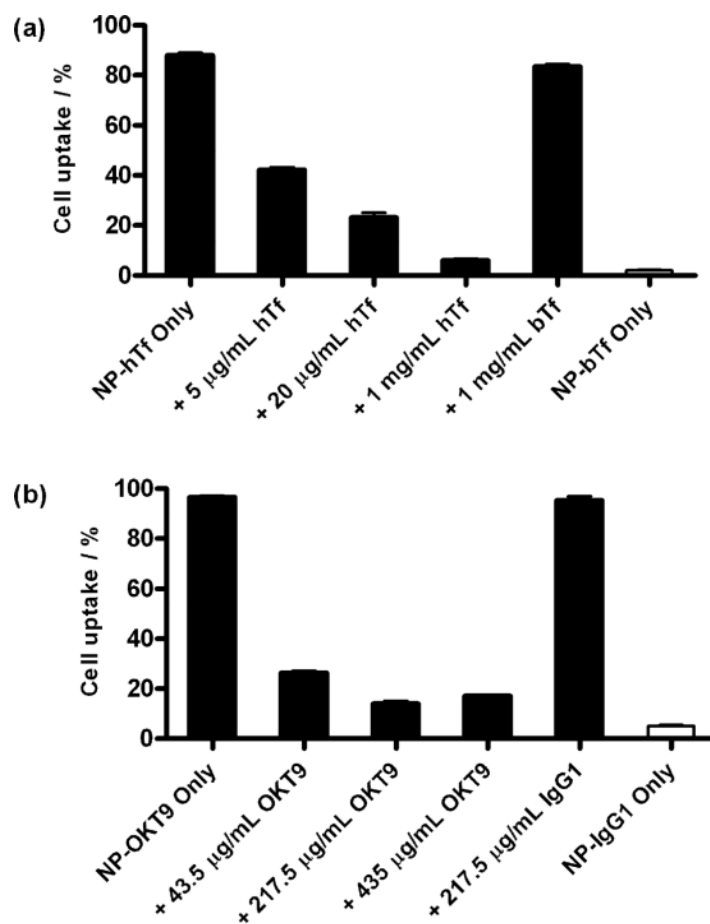
Figure 5.
Inhibition of cell uptake on Ramos cells by free targeting ligands. (a) Ramos cell uptake of human transferrin targeted PRINT NPs (NP-hTf) in the presence of free human transferrin or bovine transferrin. Bovine transferrin conjugated PRINT NPs (NP-bTf) was used as a control. (b) Ramos cell uptake of TfR monoclonal antibody OKT9 targeted PRINT NPs (NP-OKT9) in the presence of free OKT9 antibody or an isotype control IgG1.
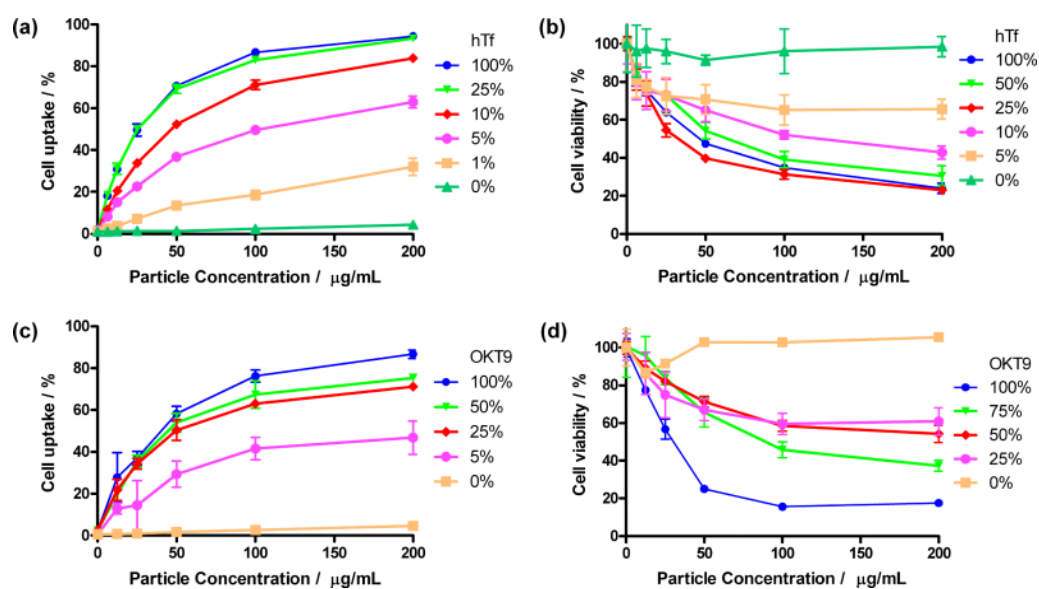
Figure 6.
Ramos cell uptake and toxicity as a function of the density of the targeting ligands (a-b) hTf and (c-d) OKT-9 on PRINT nanoparticle surface. The targeting ligand density on the PRINT NP surface was varied by substituting the targeting ligands (i.e. hTf or OKT9) with their corresponding control ligands (i.e. bTf or IgG1). (a) NPs with different hTf densities (0 %, 1 %, 5 %, 10 %, 25 % and 100 %) were incubated with Ramos cells for 4 h and the percentage of cells with internalized NPs were determined by flow cytometry. (b) NPs with different hTf densities (0 %, 5 %, 10 %, 25 %, 50 % and 100 %) were incubated with Ramos cells for 72 h and the cell viability was determined by MTS assays. (c) A similar experiment as in (a) was performed with NP-OKT9 by varying the OKT9 density (0 %, 5 %, 25 %, 50 % and 100 %). (d) A similar experiment as in (b) was performed with NP-OKT9 by varying the OKT9 density (0 %, 25 %, 50 %, 75 % and 100 %).
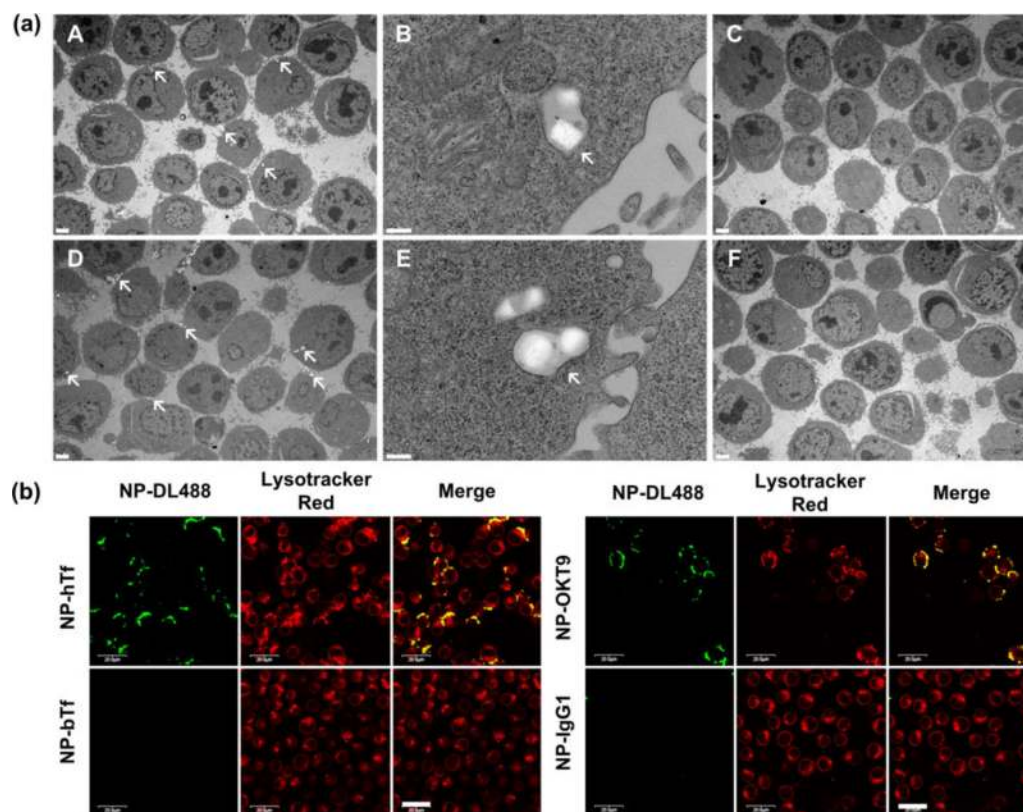
Figure 7.
Intracellular location of transferrin receptor-targeted PRINT nanoparticles in Ramos cells.
(a) Transmission electron micrographs of Ramos cells treated with TfR-targeted NPs.
Internalization of NPs in Ramos cells was observed when the cells were treated with NP-hTf
(panel A and B) or NPOKT9 (panel D and E). Little internalization was observed with NP-
bTf (panel C) or NP-IgG1 (panel F). NPs are identified by arrows. Scale bars: A, C, D and
F: 2 μm; B and E: 200 nm. (b) Internalization of TfR-targeted PRINT NPs into low pH
vesicles. Ramos cells were dosed with 50 μg/ml NPs (DyLight 488 labeled, green) for 4 h
and 100 nM lysotracker DND-99 (red) for 2 h at 37°C. Cells were then washed and imaged
with laser scanning confocal microscope. Scale Bars: 20 μm. The yellow color indicates
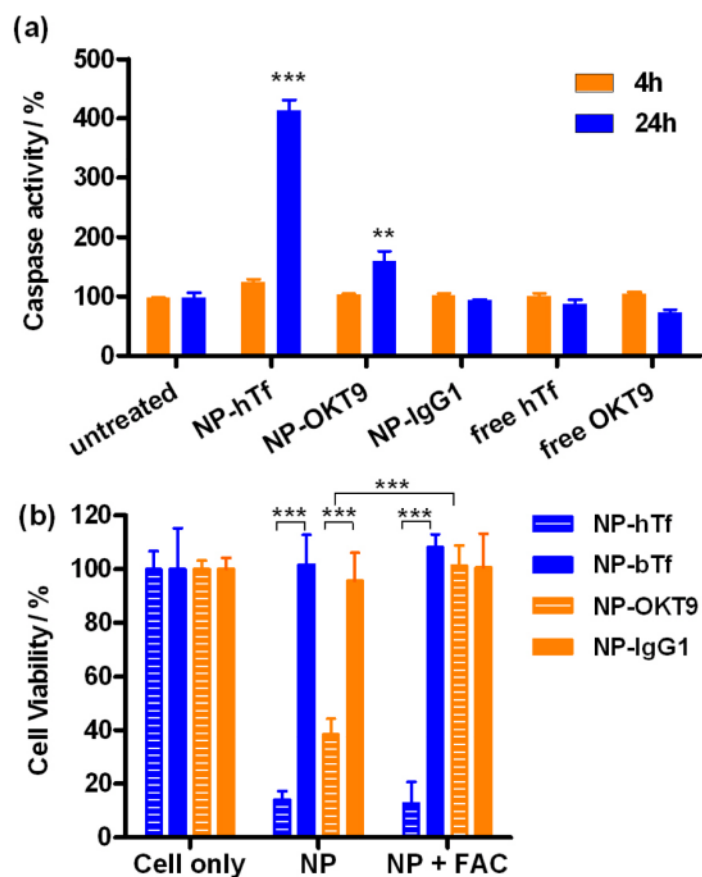colocalization of particles with lysotracker red dye.

Figure 8.
Apoptosis induced by TfR-targeted PRINT nanoparticles. (a) Caspase 3/7 activity. Ramos cells were incubated with particles (all 200 µg/mL), free hTf (20 µg/mL) or free OKT-9 (40 µg/mL) for 4 h (orange bars) or 24 h (blue bars) at 37°C. Caspase 3/7 activity was then measured with an assay kit. (b) Differential effect of iron supplementation on cytotoxcity of TfR-targeted particles. Ramos cells were dosed with PRINT NPs (200 µg/mL) in the absence or presence of ferric ammonium citrate (30 µM) for 4 h at 37°C. After another 72 h incubation in complete growth medium, cell viability assay was performed. ***, $P < 0.001$; **, $P < 0.01$.

Table 1

Characterization of PRINT Nanoparticles[a]

	Diameter[b] / nm	PDI[c]	ζ-potential[d] / mV	Surface Characterization[e]
NP-NH$_2$	287 ± 32	0.015	39.9 ± 1.7	1.2×10^6 amines per NP
NP-Mal	292 ± 76	0.080	-26.8 ± 0.3	9.3×10^4 PEG per NP
NP-hTf	287 ± 98	0.118	-31.3 ± 0.4	1.2×10^3 hTf per NP
NP-bTf	271 ± 80	0.108	-31.3 ± 0.7	1.2×10^3 bTf per NP
NP-Bio	289 ± 36	0.022	-28.9 ± 0.5	N/A
NP-Avi	267 ± 49	0.041	7.7 ± 0.7	2.1×10^3 avidin per NP
NP-OKT9	288 ± 143	0.246	-33.4 ± 1.2	1.2×10^3 OKT9 per NP
NP-IgG1	291 ± 88	0.105	-35.6 ± 1.3	1.2×10^3 IgG1 per NP

[a]NP-NH$_2$: The fabricated NPs directly from the PRINT process described in the experimental section, which has surface amine functionalities; NP-Mal: NP-NH$_2$ postfunctionalized with maleimide-PEG$_{5000}$-NHS; NP-hTf: NP conjugated with hTf; NP-bTf: NP conjugated with bTf; NP-Bio: NP-NH$_2$ postfunctionalized with biotin-PEG$_{2000}$-NHS; NP-Avi: avidinated NP by incubating NP-Bio with UltraAvidin; NP-OKT9: NP conjugated with transferrin receptor monoclonal antibody OKT9; and NP-IgG1: NP conjugated with the isotype control IgG1.

[b]Hydrodynamic diameter measured by dynamic light scattering. The average hydrodynamic diameters were obtained from ten measurements. The error bars are the half-width of the effective diameters.

[c]Polydispersity Index from the dynamic light scattering measurements.

[d]Zeta potential was measured by Zetasizer. The error bars are standard deviations from three measurements.

[e]The surface functional groups or targeting ligands were quantified by a series of assays described in the experimental section.